Middle- and High-Latitude Mesosphere and Lower Thermosphere Mean Winds and Tides in Response to Strong Polar-Night Jet Oscillations

J. Federico Conte[1] , **Jorge L. Chau[1]** , and **Dieter H. W. Peters[1]**

[1]Leibniz Institute of Atmospheric Physics, University of Rostock, Kühlungsborn, Germany

Abstract The dynamical behavior of the mesosphere and lower thermosphere (MLT) region during strongly disturbed wintertime conditions commonly known as polar-night jet oscillations (PJOs) is described in detail and compared to other wintertime conditions. For this purpose, wind measurements provided by two specular meteor radars located at Andenes (69°N, 16°E) and Juliusruh (54°N, 13°E) are used to estimate horizontal mean winds and tides as an observational basis. Winds and tidal main features are analyzed and compared for three different cases: major sudden stratospheric warming (SSW) with (a) strong PJO event, (b) non-PJO event, and (c) no major SSWs. We show that the distinction into strong PJOs, non-PJOs, and winters with no major SSWs is better suited to identify differences in the behavior of the mean winds and tides during the boreal winter. To assess the impact of the stratospheric disturbed conditions on the MLT region, we investigate the 30-year nudged simulation by the Extended Canadian Middle Atmosphere Model. Analysis of geopotential height disturbances suggests that changes in the location of the polar vortex at mesospheric heights are responsible for the jets observed in the MLT mean winds during strong PJOs, which in turn influence the evolution of semidiurnal tides by increasing or decreasing their amplitudes depending on the tidal component.

1. Introduction

The mesosphere and lower thermosphere (MLT) composes the region of the terrestrial atmosphere that spans from approximately 50 to 110 km of altitude. Understanding its behavior is of great importance to explain the coupling between the troposphere/stratosphere and the ionosphere/thermosphere regions. This coupling can be accomplished via vertical propagation of waves of different periods and scales. Planetary waves (PWs) are global-scale waves with periods of up to 30 days that are usually triggered by land-sea discontinuities and baroclinic instabilities (e.g., McCormack et al., 2014; Rossby, 1939). Thermal tides are also global-scale waves, but with periods that are subharmonics of one solar day, typically 24, 12, and 8 hr. They result from thermal forcing mainly due to absorption of solar radiation by water vapor in the troposphere and ozone in the stratosphere (e.g., Forbes, 1984). Tidal waves can also be excited by gravitational forces, as it is the case of the lunar tide (Lindzen & Chapman, 1969). Inertia gravity waves (IGWs) are middle-scale waves with typical periods of a few hours that can be generated by the orography, dynamic shear instabilities, convection, Rossby wave breaking, etc. (e.g., Fritts & Alexander, 2003; Zülicke & Peters, 2008). The vertical propagation of all these waves strongly depends on the zonal wind in the stratosphere (e.g., Holton, 2004; Yiğit & Medvedev, 2015). This implies that changes in the winds may easily facilitate or prevent the waves from propagating further upward.

Sudden stratospheric warming (SSW) events are atmospheric phenomena characterized by a rapid and pronounced increase of the temperature in the wintertime polar stratosphere that is accompanied by a deceleration or reversal from eastward to westward of the zonal mean zonal wind (ZMZW) in the stratosphere (Butler et al., 2017; Zülicke et al., 2018, and references therein). They result mainly from angular momentum deposition into the mean flow by breaking of amplified PWs that propagate upward from the troposphere region (Matsuno, 1971). The warming in the stratosphere is accompanied by a cooling in the mesosphere and a thermospheric warming, especially at middle and high latitudes (e.g., Goncharenko & Zhang, 2008). At low latitudes, the influence of SSWs manifests as enhanced variability in ionospheric parameters such us vertical plasma drift velocities and electron densities (e.g., Chau et al., 2009; Fejer et al., 2010).

According to the World Meteorological Organization (Andrews et al., 1987), SSWs can be categorized as minor or major warmings depending on the extent and amplitude of the deceleration of the ZMZW at 60°N and 10 hPa. Events characterized by a complete reversal of the ZMZW are termed as major sudden stratospheric warmings (MSSWs), while a minor warming corresponds to the case when the zonal mean zonal wind decelerates without reversing its direction (e.g., Charlton & Polvani, 2007). Some studies have suggested that the response to major SSWs of different parts of the atmosphere depends mostly on the persistence of the major warming conditions rather than on their strength (e.g., Baldwin & Dunkerton, 1999; Runde et al., 2016). Certain major SSWs are followed by anomalously warmer stratospheric conditions that can persist for longer periods of time and propagate downward, reaching the troposphere and significantly impacting its behavior (e.g., Kuroda & Kodera, 2004). This type of event is commonly referred to as polar-night jet oscillation (PJO) and occurs after roughly half of all MSSWs (e.g., Hitchcock et al., 2012). PJOs can also be observed in the mean winds in the stratosphere, where the oscillation first starts with eastward winds that reverse direction into strong westward that later on become eastward again and continue blowing in this direction for up to 2 months. Peters et al. (2018) introduced a more thorough distinction into strong, intermediate, and non-PJO events, in which strong PJOs (sPJOs) correspond to those events exceeding a three standard deviations confidence level.

Several studies have focused on identifying changes in the stratospheric conditions during major sudden warming events based on how strongly the polar vortex is distorted. Correspondingly, a MSSW is classified into either a displacement or a split event (e.g., Mitchell et al., 2013). In the first case, the polar vortex is moved away from the pole toward lower latitudes, while the second case is characterized by a splitting of the polar vortex into two pieces that is usually associated with enhanced activity of PWs with Wave Number 2. So far, there is no preferred occurrence between split and displacement events during sPJOs (e.g., Karpechko et al., 2017).

Given that the definition of sPJO is well suited to describe the evolution of the meteorological state of the stratosphere after the onset of a major sudden warming, we hypothesize that the mean winds and tides in the MLT region should exhibit clear and distinctive responses depending on the development or not of a sPJO. Consequently, we set to investigate the behavior of the MLT mean winds and tides during sPJOs, in comparison to other winter conditions. The paper is organized as follows. In section 2, we describe the technique employed to extract mean winds and tides from meteor radar measurements, and we explain the procedure used to identify sPJO events. In section 3 we present our main results, which are discussed in section 4. We finalize with the conclusions in section 5.

2. Data Analysis

The specular meteor radars (SMRs) located at the sites of Andenes (69.3°N, 16°E) and Juliusruh (54.6°N, 13.3°E) have been extensively used to study neutral winds and atmospheric waves in the MLT region (e.g., Chau et al., 2015; Hoffmann et al., 2007, 2010; Conte et al., 2017, 2018; Wilhelm et al., 2017). Combined, they provide continuous measurements for a set that is currently comprised of more than 15 years worth of data. To obtain the wind information, these measurements can be processed using various techniques. Particularly, after applying a modified version of the all-sky fit method developed by Hocking et al. (2001), hourly zonal and meridional winds can be retrieved every 2 km in the range between 75 and 105 km of altitude (Stober et al., 2017, 2018). These winds are then further processed to determine mean winds and tides. Thus, assuming that the observed winds result from the superposition of a mean background value and different period oscillations, one can fit the following expression:

$$[u, v] = [U_0, V_0] + \sum_{i=1}^{4} A_{[u,v]_i} \cos\left(2\pi \frac{(t - \phi_{[u,v]_i})}{T_i}\right), \tag{1}$$

to the retrieved zonal and meridional winds, u and v respectively. U_0 and V_0 are the mean zonal and meridional winds; $A_{[u,v]_i}$ and $\phi_{[u,v]_i}$ are the amplitude and phase, respectively, of the zonal and meridional tidal components; T_i is the period of each considered tide ($T_1 = 24$ hr, $T_2 = 12$ hr, $T_3 = 8$ hr, and $T_4 = 12.42$ hr, for the solar diurnal, solar semidiurnal, solar terdiurnal, and quasi-lunar semidiurnal tides, respectively); and t is the time in hours. Finally, u and v are independently fitted with equation (1) in bins of 21 days shifted by 1 day using a least squares technique. The selected length of the fitting window allows separating the

Table 1
*Diagnostic of the NAM-CD and PJO Events Based on ERA-Interim (Adapted From Peters et al., 2018)*

Boreal winter season	Major SSW	NAM-CD	Strong PJO	Intermediate PJO	Non-PJO	S/D
1979/1980	Yes (1)	3/1/1980			1	D
1981/1982	Yes (2)	1/25/1982			2	D
1983/1984	Yes (3)	2/25/1984		1		D
1984/1985	Yes (4)	12/31/1984	1			S
1986/1987	Yes (5)	1/23/1987	2			D
1987/1988	Yes (6)	12/7/1987	3			S
1988/1989	Yes (7)	2/19/1989	4			S
1991/1992	Yes (8)	1/18/1992			3	D
1994/1995	Yes (9)	2/4/1995			4	D
1997/1998	Yes (10)	1/7/1998		2		D
1998/1999	Yes (11)	12/16/1998	5			D
1998/1999	Yes (12)	2/26/1999		3		S
2000/2001	Yes (13)	2/7/2001		4		S
2001/2002	Yes (14)	12/28/2001			5	D
2002/2003	Yes (15)	1/18/2003			6	S
2003/2004	Yes (16)	1/4/2004	6			D
2005/2006	Yes (17)	1/21/2006	7			D
2007/2008	Yes (18)	2/22/2008			7	D
2008/2009	Yes (19)	1/23/2009	8			S
2009/2010	Yes (20)	1/28/2010			8	S
2012/2013	Yes (21)	1/7/2013	9			S
2016/2017	Yes (22)	1/29/2017			9	D
Total	22		9	4	9	

Note. S/D: split/displacement event. The missing winter seasons correspond to years with no major sudden stratospheric warmings (16 in total). NAM-CD = Northern Annular Mode central day; PJO = polar-night jet oscillation; SSW = sudden stratospheric warming.

semidiurnal solar (12 hr) and quasi-lunar (12.42 hr) tides but implies assuming that the phase and tidal amplitudes do not change much within the entire selected time interval (e.g., Chau et al., 2015). We implemented the fitting technique instead of Fourier or wavelet analysis in order to avoid the inconveniences introduced by data gaps.

In this work, we are interested in studying the different responses the MLT region may exhibit after MSSW events. Hence, it follows that one must first identify the winters in which these phenomena were observed. For this purpose, geopotential height (GPH) anomalies determined from ERA-Interim reanalysis were integrated over the northern polar cap (north of 60°N) in order to calculate the Northern Annular Mode (NAM) index (e.g., Dee et al., 2011). Specifically, GPH anomalies are obtained after subtracting the daily climatology of the selected time period. Then, the GPH anomalies are integrated north of 60°N and multiplied by −1. The NAM index is finally obtained after normalizing by the standard deviation at each pressure level (e.g., Siegmund, 2005). A major SSW event is thus identified when the NAM index crosses a threshold value of −2.3 at 10 hPa (Peters et al., 2018). The crossing also determines the central day (CD) of the MSSW. The selected threshold value yields a CD very close to the CD determined by the reversal of the mean zonal wind (e.g., Charlton & Polvani, 2007). The implementation of this criterion resulted in a total of 22 major SSWs between the years of 1980 and 2017 (see Table 1).

To examine the behavior of the stratosphere after the onset of a major SSW, we followed the PJO definition updated by Peters et al. (2018). First, principal component analysis is applied to temperature anomalies obtained from ERA-Interim reanalysis for the period 1980–2017. The anomalies are integrated over the region north of 70°N and then projected onto the first two leading empirical orthogonal functions, thus obtaining the series PC1 and PC2, which explain around 90% of the total variance. Second, in the phase space
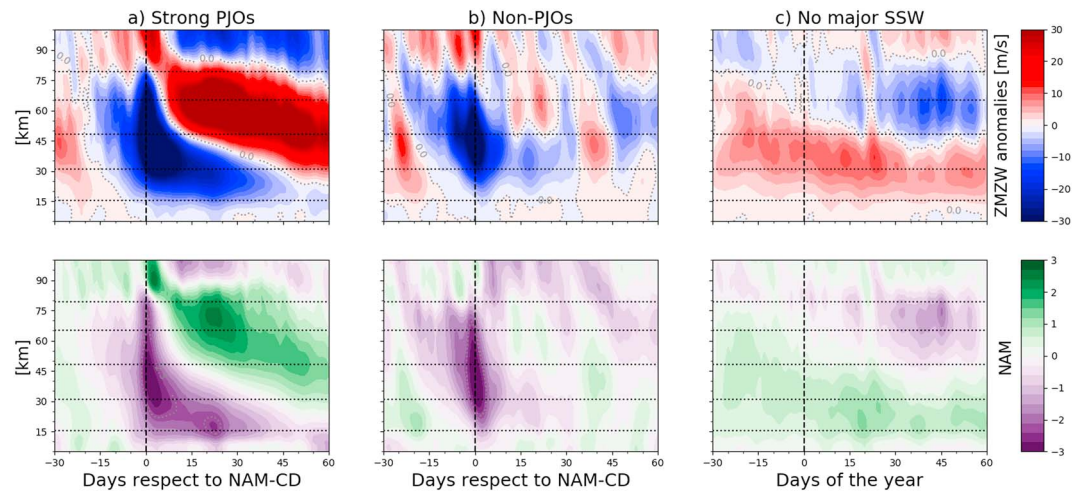
Figure 1. ZMZW anomalies and NAM index obtained from the Extended Canadian Middle Atmosphere Model. The black vertical dashed line indicates the NAM CD in (a) and (b) and 1 January in (c). The black dotted horizontal lines correspond approximately to 100, 10, 1, 0.1, and 0.01 hPa. NAM-CD = Northern Annular Mode central day; PJO = polar-night jet oscillation; SSW = sudden stratospheric warming; ZMZW = zonal mean zonal wind.

of PC1 and PC2, daily values of the amplitude $R = \sqrt{PC1^2 + PC2^2}$ and the phase angle $\theta = \arctan(PC2/PC1)$ are calculated for the entire winter season, that is, for the months between November and March. Finally, a sPJO event is defined when $R \geq 3\sigma$ and $\Delta\theta \geq 100°$, σ being the standard deviation of R. An intermediate PJO event happens if $2\sigma \leq R < 3\sigma$ and $\Delta\theta \geq 100°$. The major SSW events which do not fit into any of the two previous categories are identified as non-PJOs. This definition allows one to clearly visualize an oscillation that the polar cap stratospheric temperatures describe during anomalously warmer conditions. Given that winds and temperature are related by the thermal wind equation, the oscillation can also be distinguished in the zonal mean zonal wind, as the winds reverse from eastward to westward, and then to eastward again within a period of approximately one month (see Figure 1, which will be discussed later). It is important to stress here that all three types of PJO events, that is, strong, intermediate, and non-PJOs occur during winters with MSSWs. For comparison purposes, winters with no major SSWs (shortly, non-MSSWs) are also investigated.

In order to assess the impact of sPJO events on the dynamics of the MLT region, we analyzed the 30-year nudged simulation by the extended Canadian Middle Atmosphere Model (Ext-CMAM30). The Ext-CMAM30 is a spectral global circulation model of the troposphere, middle atmosphere, and lower thermosphere that vertically extends up to ~210 km. It includes interactive ozone chemistry, as well as observed and projected forcing of the atmosphere by greenhouse gases emissions and ozone-depleting substances (e.g., de Grandpré et al., 2000; McLandress, 1997). The tropospheric and stratospheric meteorological states are nudged toward ERA-Interim reanalysis data sets (e.g., McLandress et al., 2014; Scinocca et al., 2008). Parameterizations of viscosity, ion drag, and orographic and nonorographic gravity wave drag have also been implemented in these simulations (e.g., Fomichev et al., 2002). The Ext-CMAM30 outputs used in this study were obtained from the website of the Canadian Centre for Climate Modelling and Analysis. Their spatial resolution is of 5.625° by 3.75° in latitude and longitude and 87 pressure levels in vertical. The temporal resolution is of 6 hr. The meteorological fields explored in Ext-CMAM30 include zonal winds, GPHs, total ozone, and ozone concentration.

The SMR data sets used in this study to investigate the MLT dynamics at high and middle latitudes cover four sPJO and four non-PJO events in the case of Andenes (2003–2017) and two sPJOs and three non-PJOs in the case of Juliusruh (2008–2017). The Ext-CMAM30 outputs span from 1980 to middle of 2010, comprising a total of nine sPJO and nine non-PJO events. Although four intermediate PJOs were recorded during 1980–2017, none of them took place within the period of time with available SMR data, that is, between the years of 2003 and 2017. Consequently, this last type of event was not considered in the present study. A summary of all the events can be found in Table 1. Note that a sPJO event not necessarily corresponds to a split event (five out of nine sPJOs are split events).
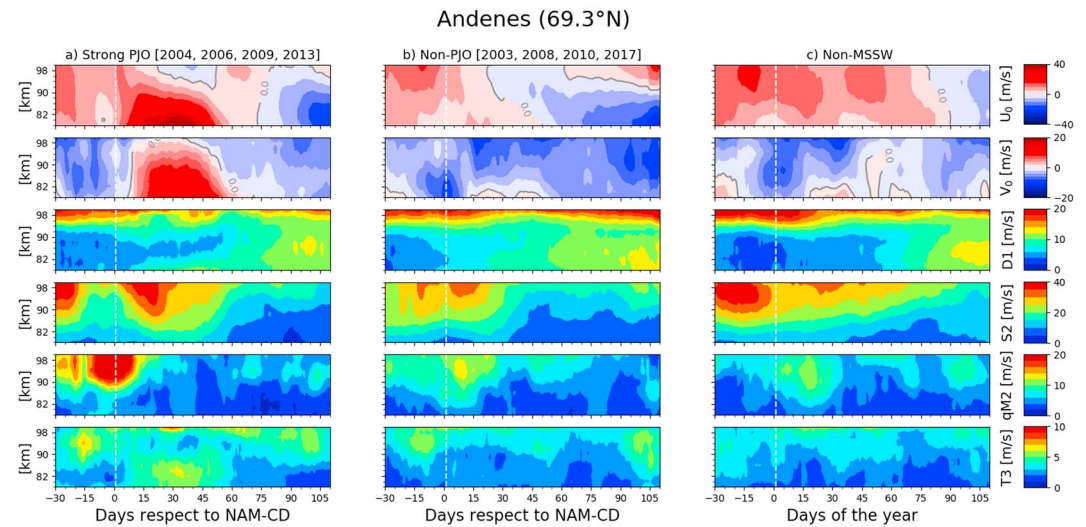
Figure 2. Composite over Andenes of the mean zonal (U_0) and meridional (V_0) winds, the diurnal and semidiurnal solar tides (D1 and S2, respectively), the semidiurnal quasi-lunar tide (qM2) and the terdiurnal solar tide (T3), for (a) strong PJO years, (b) non-PJO years, and (c) years with no MSSW. Zero-wind contours in U_0 and V_0 are presented. The vertical white dashed line indicates the reference day: the NAM-CD in (a) and (b) and 1 January in (c). MSSW = major sudden stratospheric warming; NAM-CD = Northern Annular Mode central day; PJO = polar-night jet oscillation.

3. Results

3.1. High Latitudes

In Figure 2 we present a composite over Andenes of the mean zonal (U_0) and meridional (V_0) winds, and the total amplitudes of the solar diurnal (D1) and semidiurnal (S2) tides, the semidiurnal quasi-lunar (qM2) tide and the terdiurnal solar (T3) tide. The composites correspond to years with (Column a) sPJO events, (Column b) non-PJO events and (Column c) non-MSSWs. The term *total amplitude* refers to the magnitude of the vector sum of the corresponding zonal and meridional components. From this figure, one can easily notice significant differences among the three cases in all six quantities. During sPJO years, the mean winds are severely affected. A strong enhancement develops in both the zonal and meridional components almost immediately after the NAM-CD and persists for about 50 days. In the case of the zonal component, there is a significant enhancement of the eastward wind, particularly at altitudes below 90 km. Above ~92 km, the mean eastward winds exhibit similar amplitudes of around 25 m/s until approximately 10 days after the NAM-CD, when they start decreasing to eventually reverse direction and blow westward. These westward winds are not able to extend to lower altitudes as it is the case during non-PJO years. The strong eastward jet taking place below ~92 km seems to prevent the descending westward winds observed at other winters from extending further down. When reaching an altitude of 92 km, they abruptly reverse direction at all heights above that level. At this point, the mean eastward winds span the entire observed height range. Approximately 1 month later, they reverse direction once again, but this time at all observed heights and at approximately the same time. This final reversal toward westward direction happens ~70 days after the NAM-CD and mainly from below, contrary to non-MSSWs when it develops mainly from above (Column c). During non-PJO years, the reversal of the mean zonal wind from eastward to westward direction happens also mainly from above, starting roughly 20 days after the NAM-CD for altitudes above 90 km to ~40 days or more after the NAM-CD for heights below 84 km. From then on, westward winds dominate at all heights until the beginning of summer, which is characterized by a wind reversal from westward below ~92 km to eastward above. The tilt of this summer reversal is less pronounced and develops approximately 40 to 50 days earlier than in the case of sPJO years and non-MSSWs.

The mean meridional winds behave very similarly during non-PJO events and non-MSSWs, blowing mainly toward the south (Columns b and c). In years with sPJO events, the main difference is observed during the two months following the NAM-CD when a strong northward jet prevails. Approximately 35 days after the NAM-CD, the northward winds start reversing direction, first at an altitude of 99 km to then progressively continue downward until southward winds dominate again at all height levels, about 2 months after the
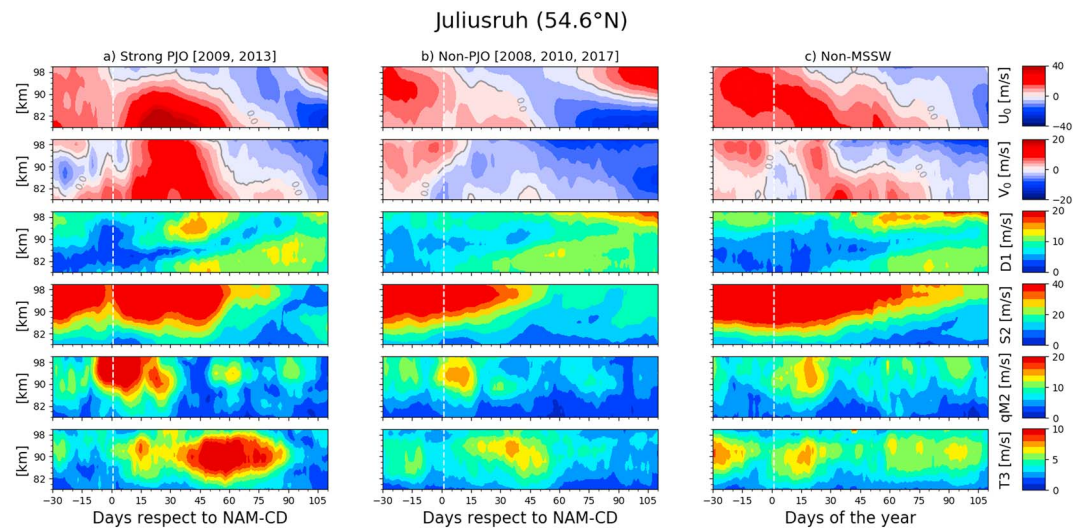
Figure 3. Same as Figure 2 but over Juliusruh.

NAM-CD. Another difference can be distinguished around the NAM-CD of sPJO years, when the mean meridional winds are almost zero at all observed altitudes. This zero-wind line is not observed in the other two cases.

Differences in the behavior of the diurnal solar tide are not as evident as in the case of the mean winds. This is not surprising given that D1 becomes less important poleward of 30° (e.g., Andrews et al., 1987). One can only notice that in early winter above ~94 km, the diurnal solar tide maximum amplitudes during non-MSSWs are larger and reach lower altitudes than in sPJO and non-PJO years.

The behavior of the semidiurnal solar tide (S2) is significantly affected during sPJO years, compared to non-PJOs and years with no MSSWs. Previous studies have reported a considerable decrease of S2 amplitudes starting 1 or 2 weeks before the onset of a major SSW (e.g.,Chau et al., 2015). A few days after the event, they recover and reach values as large as (or even larger than) those observed before the pre-MSSW decrease (e.g., Siddiqui et al., 2018). Figure 2, however, shows that only in years with sPJO events the aforementioned behavior of the S2 tide is observed. The decrease is very pronounced and extends for about 15 days. A few days after the NAM-CD, S2 amplitudes start recovering until they reach again values of ~40 m/s. During non-PJO years, there is some decrease of the S2 amplitudes around the NAM-CD, but above ~94 km. After the NAM-CD, the S2 amplitudes slightly increase only above ~97 km. During the winter of years with no major SSWs, the S2 tide exhibits larger amplitudes and extends for about one more month than during non-PJO years. With respect to sPJO years, the S2 amplitudes during wintertime are smaller, but they also extend for longer periods of time (~15 more days).

The semidiurnal quasi-lunar tide exhibits similar amplitudes except in the case of sPJO years, when significantly larger amplitudes can be observed during an interval of approximately 40 days around the NAM-CD, although with some intermittence between 30 and 15 days prior to the NAM-CD. These amplitudes reach values of 20 m/s and are the largest among the three cases analyzed in this study. They develop above ~90 km at about the same time the S2 tide starts decreasing and maintain for 20 days to then abruptly decrease and become negligible during the rest of the year. During the 20 days following the day of reference, the qM2 tide of non-PJO years shows slightly larger amplitudes (~5 m/s) than that of non-MSSWs. However, in years with no major SSWs the qM2 tide shows a minor enhancement in the spring, a time of the year with no qM2 activity in the other two cases.

The maximum amplitudes of the terdiurnal solar tide (10 m/s) are observed during sPJO years, above 90 km ~15 days before the NAM-CD and below 88 km 30 days after the NAM-CD. This second maximum constitutes the peak of an interval of larger T3 amplitudes that develops 15 days after the NAM-CD and persists for about 30 days, coinciding with the time period when the eastward and northward jets are observed in the mean zonal and meridional winds, respectively. In the case of non-PJO years, some weak activity of T3 can be detected before the NAM-CD and in the spring. In non-MSSWs, the T3 tide is extremely weak.

Table 2
Summary of the Main Differences Between the Mean Winds and Semidiurnal Tides of Strong PJOs and the other Two Cases

	High latitudes (Andenes)		Middle latitudes (Juliusruh)	
Parameter	Strong PJO	Non-PJO/Non-MSSW	Strong PJO	Non-PJO/Non-MSSW
U_0	Strong eastward jet for about 50 days, starting a few days after the NAM-CD	Weak eastward winds and a reversal to westward mainly from above	Strong eastward jet for about 50 days, starting immediately after the NAM-CD	Weak eastward winds and a reversal to westward mainly from above
V_0	Strong northward jet for about 50 days, starting a few days after the NAM-CD	Southward winds dominate before and after the NAM-CD	Strong northward jet for about 50 days, starting a few days after the NAM-CD	Southward winds dominate after the NAM-CD
S2	Pronounced decrease during the two weeks prior to the NAM-CD. Recovery after the NAM-CD	Similar amplitudes before, during and after the NAM-CD	Decrease during 2–3 days prior to the NAM-CD	Same amplitudes before, during and after the NAM-CD
qM2	Strong amplitude enhancement during 25–30 days around the NAM-CD	Very weak amplitude increase, and only after the NAM-CD	Strong amplitude enhancement during 25–30 days around the NAM-CD	Amplitudes increase only after the NAM-CD, and sustain for a shorter period of time

Note. MSSW = major sudden stratospheric warming; NAM-CD = Northern Annular Mode central day; PJO = polar-night jet oscillation.

3.2. Middle Latitudes

Figure 3 shows similar composites as Figure 2 but over Juliusruh. A visual inspection of this figure reveals that the main difference with respect to Andenes lies in the amplitudes, which in general are at least 10% larger than at high latitudes. A strong eastward (northward) jet develops in the mean zonal (meridional) wind immediately (roughly 5 days) after the NAM-CD of sPJO years. It happens at all height levels in the meridional component but only below ∼96 km in the zonal component. Above 96 km, the mean zonal wind reverses direction to westward 1 day before the NAM-CD. Approximately 2 months after the NAM-CD, this reversal starts descending to lower altitudes until all observed heights are dominated by westward winds. During both non-PJOs and non-MSSWs the reversal to westward winds happens mainly from above but approximately 10 days earlier in the case of non-PJO years. These two cases exhibit another reversal to westward winds during the fall. It occurs above ∼94 km and lasts for about 10 days (not shown). The differences in the meridional wind among the three cases are similar to those observed over Andenes: sPJO years exhibit a strong enhancement in the northward direction that lasts almost 60 days, starting a few days after the NAM-CD. Below ∼85 km, the northward meridional winds decelerate but do not reverse direction until roughly 95 days after the NAM-CD. During non-PJO years, the northward winds dominate mainly before the NAM-CD, spanning all altitudes until ∼10 days before the NAM-CD. In the case of non-MSSWs, northward meridional winds dominate before 1 January. Below ∼96 km, they reverse direction around this day to later on become northward again and blow in this direction for about 20 (60) days above (below) 90 km of altitude. From then on, southward winds dominate until late fall.

Similarly to high-latitude locations, the diurnal solar tide over Juliusruh does not show many considerable differences among all three cases. Only one noticeable difference is observed, approximately 30 days after the NAM-CD of sPJOs, when an enhancement of D1 develops and maintains for about 20 days, starting first at ∼92 km to later on extend to higher altitudes.

The decrease of the S2 tide around the NAM-CD during sPJO years lasts a much shorter time in comparison to high latitudes. The S2 tide amplitudes slightly decrease above ∼94 km for only a couple of days to then recover to their previous values of more than 40 m/s. Approximately between 87 and 93 km of altitude, the decrease is more clear and lasts for about a week. Non-PJO years do not show any sort of decrease of the S2 tide around the NAM-CD. The same happens in the case of non-MSSWs, but with one noticeable difference: strong S2 amplitudes are observed for at least 30 more days than during non-PJO years.

In the case of sPJO years, the semidiurnal quasi-lunar tide over Juliusruh is mainly active around the NAM-CD for about 1 month. During non-PJOs and non-MSSWs, there is an enhancement of qM2 after the reference day, although it develops approximately 15 days later in the case of years with no major SSWs. Similarly to high latitudes, the most noticeable difference in the behavior of the qM2 tide is that during sPJO years it is significantly enhanced around the NAM-CD. This enhancement occurs above 88 km roughly 10 days before the NAM-CD and lasts for almost 30 days. During this interval of time, qM2 amplitudes can reach

values of up to 25 m/s, which is equivalent to ∼50% of the S2 amplitude during that same period. This is not the case during non-PJO years, which might be indicating that not all major SSWs can trigger a strong qM2 enhancement but only those characterized by extremely disturbed wind conditions, that is, sPJO events.

As it has been the case in all other five quantities, the amplitudes of the terdiurnal solar tide are considerably larger over Juliusruh compared to Andenes. From Figure 3, one can see that the T3 tide shows significant activity mainly after the NAM-CD for strong and non-PJO years, as well as before and after the reference day for non-MSSWs. In sPJO years, T3 exhibits the largest maximum amplitudes (∼15 m/s). These large amplitudes develop around 90 km of altitude and then extend further up and down until they span from ∼82 up to 96 km of height. Once this enhancement disappears, a period of about 20 days with almost no T3 tidal activity follows. A similar pattern is observed during non-PJO years, but in this case the enhancement is not as pronounced and maintains for a shorter period of time. The T3 tide of years with no MSSWs exhibits three enhancements in its activity. The first one during the first 2 weeks of December, the second roughly one week after 1 January, and a last one during March.

To underline the fact that only the dynamics of sPJOs exhibits significant differences with respect to other wintertime conditions, a summary of the main distinctive features characterizing mean winds and the semidiurnal solar and quasi-lunar tides during sPJOs and the other two cases (non-PJOs and non-MSSWs) is presented in Table 2, for both high and middle latitudes.

4. Discussion

A great amount of studies have focused on the response of the MLT to dynamically disturbed conditions, particularly to SSW events (e.g., Charlton & Polvani, 2007; Forbes & Zhang, 2012; Fuller-Rowell et al., 2010; Jacobi et al., 2003; Limpasuvan et al., 2016; Matthias et al., 2013; Zhang & Forbes, 2014). The conditions of the polar vortex at stratospheric altitudes during SSWs have also been extensively investigated (e.g., Harvey et al., 2002; Manney et al., 1994; Mitchell et al., 2011; Waugh & Randel, 1999). Recently, Harvey et al. (2018) extended the analysis of the polar vortex wintertime climatology to the mesosphere region. However, to the best of our recollection, the boreal MLT mean winds and tides obtained from meteor radar measurements have not been analyzed with respect to different manifestations of MSSWs, and in particular to sPJO events. sPJO events refer to a long-lasting recovery phase of the polar stratosphere from major warming conditions (e.g., Kodera et al., 2000). Figure 1 shows this effect very clearly. In the phase after the NAM-CD, and for a time interval that may last up to 2 months, strong westward ZMZW anomalies (i.e., the ZMZW minus the climatology, averaged between 50°N and 70°N) slowly propagate downward from the stratosphere into the upper troposphere. A similar pattern can be distinguished in the NAM index. Non-PJO years also show strong westward ZMZW anomalies and the NAM index values cross the −2.3 threshold, something expected given that non-PJO events occur after major stratospheric warmings as well. However, the downward propagating pattern after the NAM-CD is not evident during this type of events. In the case of years with no major SSWs (Column c), the slightly downward propagating variability detected in the ZMZW anomalies and, to a lesser extent, in the NAM index may be due to minor warmings or simply a result of the mean seasonal cycle. Thus, we expect from our hypothesis a clear separation in the MLT behavior between sPJOs and the other two cases.

Figures 2 and 3 show that the situation in the MLT region is quite different depending on the development or not of a sPJO, at least at the locations of Andenes and Juliusruh. The mean zonal eastward wind indeed decelerates around the NAM-CD of sPJOs, but it recovers very rapidly and enhances significantly in a matter of a few days. This strong enhancement persists for more than 40 days and coincides with a strong poleward jet in the mean meridional wind, which might be indicating that the edge of the polar vortex at upper mesosphere altitudes crosses over northern Europe during this type of events. Previous studies have shown that the polar vortex at stratospheric altitudes is located more toward the North Atlantic European sector during sPJO events. In the case of non-PJO events, it tends to stay mainly over the North Pacific region (e.g., Peters et al., 2018). GPH disturbances derived from the Ext-CMAM30 (obtained after subtracting the zonal mean, and also referred to as eddy GPH; e.g., Harvey et al., 2018) indicate that the location of the polar vortex in the mesosphere is different from that in the stratosphere. This can be appreciated in Figure 4, where we present composites at 100, 10, 1, 0.1, and 0.01 hPa of the GPH disturbances averaged over 15 days after the reference day of the three cases here studied (NAM-CD for both types of PJOs and 1 January in the case of non-MSSWs). Although the Ext-CMAM30 is free running above 1 hPa, McLandress et al. (2013) showed
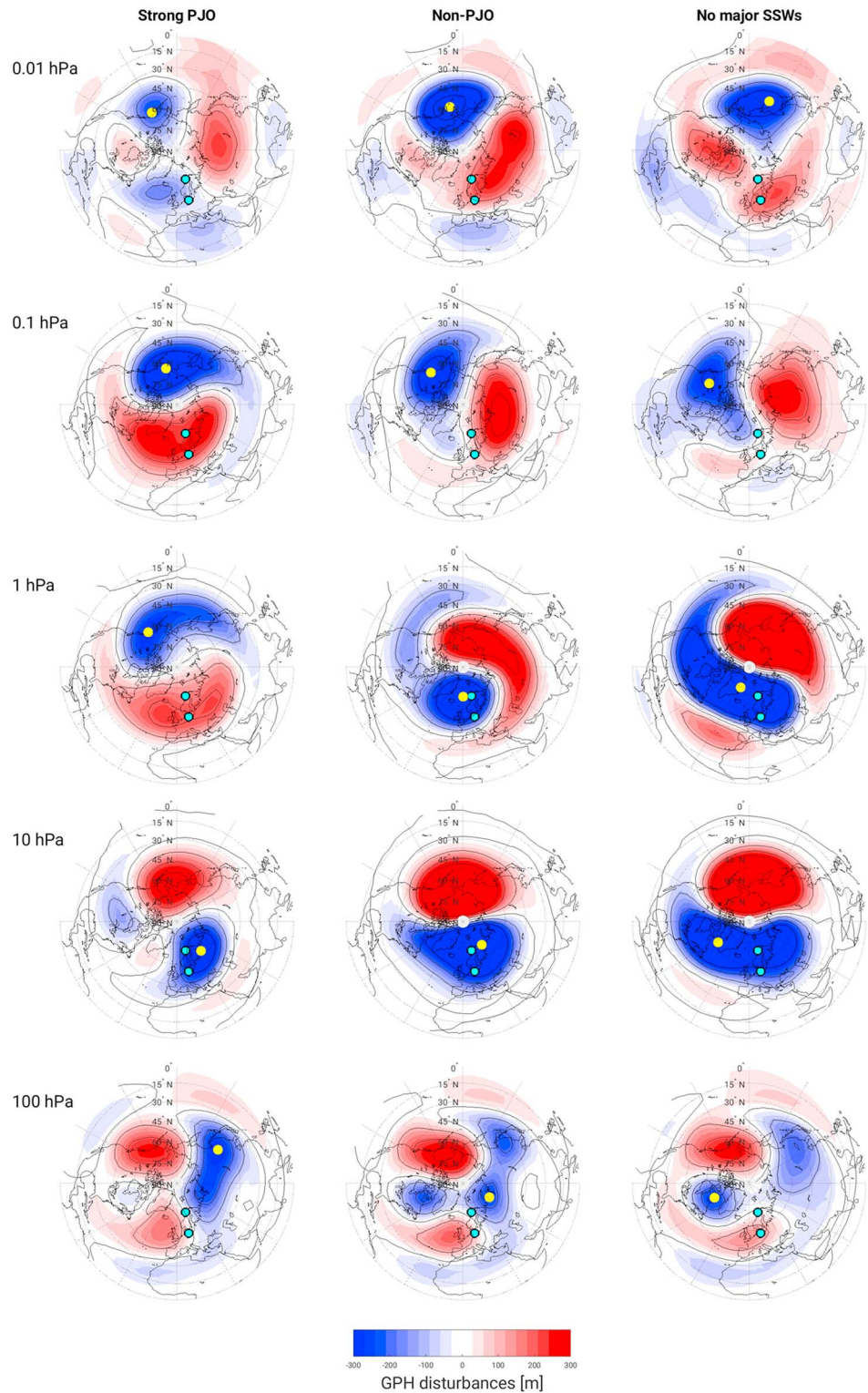
Figure 4. Extended Canadian Middle Atmosphere Model GPH disturbances averaged over 15 days after the reference day of strong PJOs, non-PJOs, and years with no major sudden stratospheric warmings, at (from bottom to top) 100, 10, 1, 0.1, and 0.01 hPa. The cyan circles indicate the location of Andenes and Juliusruh. The yellow circle indicates the absolute minimum. GPH = geopotential height; MSSW = major sudden stratospheric warming; NAM-CD = Northern Annular Mode central day; PJO = polar-night jet oscillation.
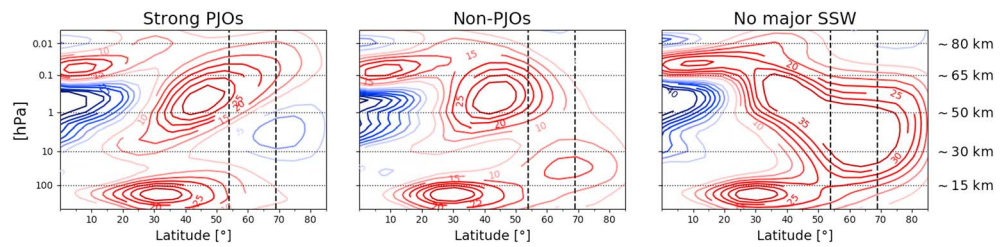
Figure 5. Contours of the zonal mean zonal wind obtained from the Extended Canadian Middle Atmosphere Model averaged over 15 days after the reference day of strong PJOs, non-PJOs, and years with no major SSWs, as a function of latitude and pressure. Contours are given in meters per second. Red positive values correspond to eastward winds, while blue negative values indicate westward winds. The black dashed vertical lines correspond to the latitude of Andenes and Juliusruh. PJO = polar-night jet oscillation; SSW = sudden stratospheric warming.

that Ext-CMAM30 data sets are in good agreement with *Aura* Microwave Limb Sounder measurements at mesospheric heights.

In the stereographic plots presented in Figure 4, one can notice that there are clear differences between sPJO events and the other two cases, especially at 1, 0.1, and 0.01 hPa. During sPJO events, GPH disturbances above Andenes and Juliusruh go through a clear transition as the altitude increases. Negative values (i.e., a GPH value below the zonal mean, also known as a cyclonic anomaly) dominate at 10 hPa and do so again at 0.01 hPa, although in this last case with weaker amplitudes. Conversely, at 100, 1, and 0.1 hPa, the region above northern Europe is dominated by positive GPH disturbances (i.e., anticyclonic anomalies), with larger values at 0.1 hPa. In the case of non-PJO events, GPH disturbances also experience changes with altitude, but these are considerably different. Small positive and negative values dominate the GPH disturbances above Andenes and Juliusruh at 100 hPa, while only negative values dominate at both 10 and 1 hPa. Higher up, the GPH disturbances become positive again, but with larger amplitudes at 0.01 hPa. During non-MSSWs, the GPH disturbances above Andenes and Juliusruh exhibit the same characteristics as in the case of non-PJOs. Thus, similarly to our SMR observations, the Ext-CMAM30 outputs also reveal that only the dynamics of sPJOs differs considerably from that of the other two cases. Non-PJOs and non-MSSWs exhibit similar characteristics.

During sPJOs, the GPH disturbances at 100 and 10 hPa reveal a weak upward propagation of PWs with Wave Number 2 (PW2). Then, from 10 to 1 hPa, a strong upward propagation of the PW with Wave Number 1 (PW1) can be noticed. The upward propagation becomes very weak above 1 hPa. However, at 0.01 hPa the PW2 pattern becomes dominant again, probably as a result of in situ generation by filtered gravity waves (e.g., Liu & Roble, 2002). Non-PJOs and non-MSSWs preserve the Wave Number 1 structure at all considered levels, except at 100 hPa where the Wave Number 2 pattern is more evident. According to Charney and Drazin (1961), PW1 structures can propagate upward only if the mean zonal wind is directed toward the east with a speed of ∼0–40 m/s. In case of the PW2 pattern, its propagation is possible if the speed of the eastward mean zonal wind is between 0 and ∼20 m/s. From Figure 5, where we present the ZMZW obtained from the Ext-CMAM30 averaged over 15 days after the reference day of the three cases considered in this study, one can notice that during non-PJOs and non-MSSWs, the ZMZW in the polar cap below 0.1 hPa is always eastward directed, with a speed of about 20 m/s. This prevents propagation of PW2 but allows PW1 structures to propagate further upward, as it can be inferred from the dominance of the PW1 pattern detected in the GPH disturbances at 0.1 hPa and above.

In the case of sPJO events, the ZMZW between 10 and 1 hPa is westward directed in the polar region, as a consequence of deceleration due to strong upward propagation of PW1 structures (see Figure 4). This feature is not evident during non-PJOs and non-MSSWs, most likely due to a stronger eastward ZMZW that prevents the PWs from further propagating (note that there is a strong upward propagation of the PW1 structure only above 1 hPa, where the eastward ZMZW is weaker). During sPJOs, the ZMZW above 1 hPa recovers and becomes eastward again, in agreement with the enhancement of the mean zonal wind observed with our SMRs (Figures 2 and 3). Besides, the recovery of the eastward ZMZW may facilitate the upward propagation of westward propagating GWs, which at higher altitudes (∼80 km) might in situ generate the PW2 structure described above (upper panels of Figure 4).
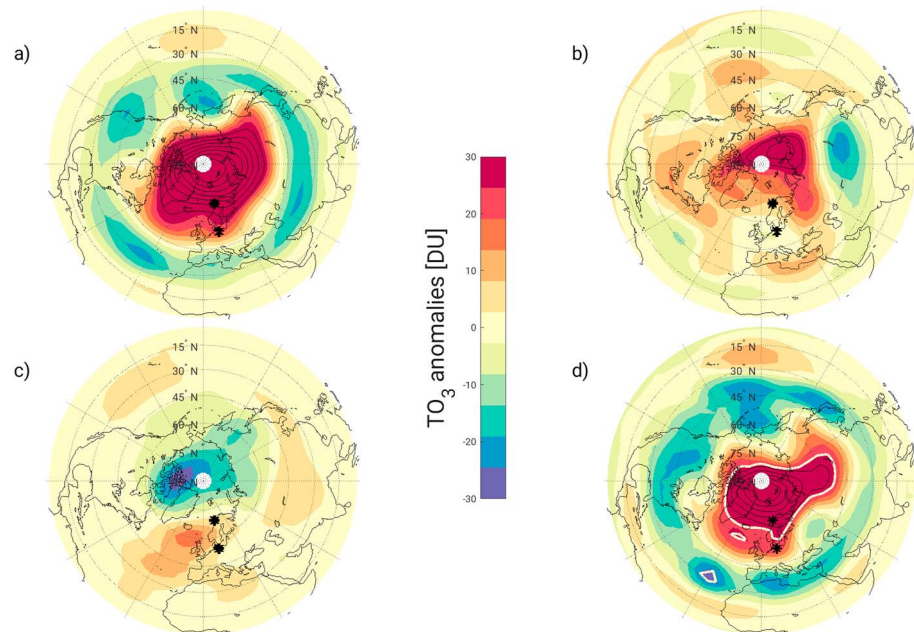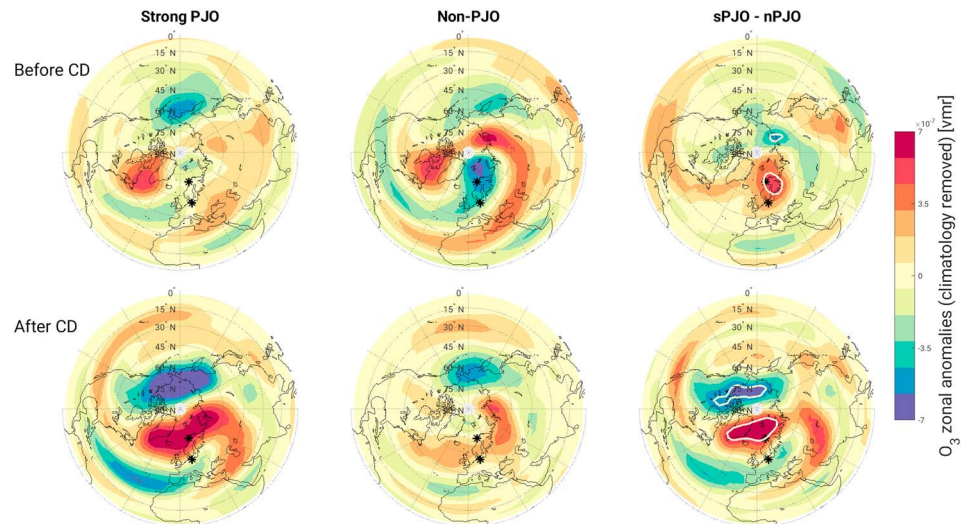
Figure 6. Extended Canadian Middle Atmosphere Model total ozone anomalies averaged over 15 days after the reference day for (a) strong polar-night jet oscillations (PJOs), (b) non-PJOs, and (c) non-major sudden stratospheric warmings. The difference between strong and non-PJO events is presented in (d). The white contours indicate the areas where the difference has a 95% of statistic significance. The color scale is in Dobson units (1 DU = 2.69×10^{20} m^{-2}). The black asterisks indicate the location of Andenes and Juliusruh.

From the results presented in section 3 (see Table 2 for a quick summary), it is clear that only during sPJO events the tides in the MLT region exhibit significant differences compared to wintertimes with no major SSWs. If a major SSW develops but the recovery phase is not sufficiently prolonged in time (i.e., during a non-PJO event), the MLT region is not considerably affected and its behavior resembles that of a winter with no major SSWs (Columns b and c in both Figures 2 and 3). Under MSSW conditions, changes in the stratospheric global circulation driven by enhanced quasi-stationary PWs lead to a more asymmetric longitudinal distribution of the stratospheric ozone, which in turn may trigger nonmigrating semidiurnal tidal components (e.g., Goncharenko et al., 2012). These nonmigrating components might interact out of phase with the migrating semidiurnal tide and eventually induce the S2 decrease observed around the NAM-CD of sPJO events. At this point, it is worth noting that the observed S2 tide studied here may be the result of both migrating and nonmigrating components, given that single point measurements do not allow us to distinguish between different wave numbers. Besides, given the 6-hr time resolution of the Ext-CMAM30 outputs, only waves with periods larger than 12 hr can be unambiguously resolved, meaning that only the diurnal tide can be studied with the Ext-CMAM30 outputs considered in this work.

sPJO events are also characterized by a period of stronger PW activity following the NAM-CD (e.g., Peters et al., 2018). This increase in the PW activity may favor a redistribution of ozone, with a strong increase over Eurasia, which in turn might allow the S2 tidal amplitudes to recover to their pre-MSSW values. Figure 6 presents Northern Hemisphere stereographic projections of the total ozone anomalies obtained from the Ext-CMAM30 for strong and non-PJO events, non-MSSWs, and the difference between the first two cases. The plots show an average over the 15 days following the reference day. The white curve encloses the area where the differences in the total ozone anomalies have a significance of 95% (using the two-tailed Student's *t* test). This area composes parts of the North Atlantic European region and Siberia, in agreement with previous studies (e.g., Butler et al., 2017; Peters et al., 2018). The largest positive and more uniformly distributed (in longitude) total ozone anomalies of sPJO events are consistent with the recovery of the observed S2 tide, specially at high-latitude locations. Besides, the area of greatest significance includes Andenes but not Julisuruh, which may partially explain why the differences in the S2 behavior between strong and non-PJO events at middle latitudes are not as pronounced as over high-latitude locations.

Figure 7. Extended Canadian Middle Atmosphere Model ozone zonal anomalies at 10 hPa averaged over 15 days (top row) before and (bottom row) after the reference day of strong PJOs and non-PJOs, and the difference between these two cases. The zonal anomalies were calculated after removing the climatology of the 30-year period. The black asterisks indicate the location of Andenes and Juliusruh. The white curves (third column) enclose the areas where the difference is 95% significant. PJO = polar-night jet oscillation; sPJO = strong PJO; CD = central day.

Figure 7 shows stereographic projections of the ozone zonal anomalies at 10 hPa averaged over 15 days before and after the reference day of sPJOs and non-PJOs, and the difference between these two types of events. From this figure, one can notice that prior to the NAM-CD of sPJOs, the ozone concentration in the stratosphere is significantly reduced over the Scandinavian Peninsula and parts of northern Germany. After the NAM-CD, the ozone concentration increases considerably, particularly over Andenes, which is consistent with the observed recovery of the S2 tide. Similarly to the case of the total ozone (Figure 6), only Andenes lies inside the area where the difference between strong and non-PJOs is 95% significant. In the case of non-PJO events (second column in Figure 7), there is a decrease/increase pattern in the ozone concentration over parts of northern Europe before and after the NAM-CD. This might be easily associated with an enhancement in the S2 tide amplitudes after the NAM-CD, which is not consistent with the observed behavior in our meteor radar measurements, where S2 shows similar amplitudes before and after the NAM-CD over Andenes, and slightly smaller after the NAM-CD over Juliusruh.

Given that changes in the mean winds can modify the amplitudes of tides (e.g., Jin et al., 2012), it is most likely that the enhanced eastward mean zonal wind observed after the NAM-CD of sPJO events is the main factor responsible for the increase in the S2 amplitudes observed during that same period. The three cases considered in this study have one clear (and obvious, from a theoretical point of view) similarity: the S2 tide exhibits significant amplitudes only when the mean zonal wind blows to the east. As soon as the mean zonal eastward winds weaken, the S2 tide amplitudes start decreasing. In the case of sPJO events, the changes the S2 tidal amplitudes experience around the NAM-CD are probably a consequence of changes in the mean winds at mesospheric altitudes. Ext-CMAM30 GPH disturbances indicate that the polar vortex area of influence at upper mesospheric heights encompasses parts of the North Atlantic European region. Particularly, the edge of the vortex at 0.01 hPa (∼80 km) crosses the region directly above Andenes and Juliusruh, which is consistent with the enhancements observed in the horizontal mean winds at these two sites.

Understanding the enhanced amplitudes of the semidiurnal quasi-lunar tide around the NAM-CD of sPJO events is more complicated. Several mechanisms have been proposed in order to explain this tidal component. Some studies have suggested that changes in temperature and in the mean winds can lead to a shifting of the atmosphere's so-called Pekeris resonance frequency toward the lunar period and a consequent enhancement of qM2 (e.g., Forbes & Zhang, 2012). This may explain the behavior of qM2 during sPJOs, but it cannot explain the differences between strong and non-PJOs events. Other studies suggest that the qM2 tide is in fact a result of nonlinear interactions between the S2 tide and quasi-stationary PWs (e.g., He et al., 2017; He & Chau, 2019). From the structure of the GPH disturbances at 0.01 hPa (Figure 4), one may argue that the PW1 pattern becomes very weak at these heights partly because of nonlinear interactions with the

S2 tide that then result in the observed enhancement of qM2. In non-PJOs and non-MSSWs, the PW1 pattern does not disappear at 0.01 hPa, which may partially explain why the qM2 is not significantly enhanced as in the case of sPJOs. However, this second mechanism cannot explain the enhancement of qM2 observed over Juliusruh after the NAM-CD of non-PJOs, neither the larger qM2 amplitudes observed during the first weeks of January in years with no major SSWs.

Fuller-Rowell et al. (2016) showed that under severely disturbed wind conditions, the phase of the S2 tide may be shifted. Given the long averaging window used in our study (21 days), the shifting of the phase could be picked up by our fitting technique as a signal of a slightly different frequency that then we interpreted as that of the lunar tide. Usage of shorter running windows (e.g., 4 days) revealed that the phase of the S2 tide indeed changes around the NAM-CD of sPJOs but that it also changes during non-PJO events (not shown here). The tidal amplitudes obtained using the 4-day running window exhibit more variability, which is expected given the shorter length of the averaging window, although the same main features as in the case of the 21-day window are observed in both the mean winds and the solar tides. Variability within a time interval of 21 days may also result in sidebands of the S2 tide that are misinterpreted as the lunar tide. However, the sidebands are usually associated with different wave numbers, which can only be resolved by combining observations from different longitudinal sectors (He & Chau, 2019). Thus, it is evident that from our analysis one cannot fully determine which one of the proposed mechanisms (or if a combination of them) is responsible for the enhanced qM2 amplitudes observed during sPJOs. Hence, the usage of the term *quasi-lunar*.

As a next step, in future studies we plan to investigate the dynamics of sPJOs using Microwave Limb Sounder measurements. Besides, we realize that detailed model studies are needed to fully understand the physics behind the enhancement of qM2 during sPJOs. A simple first step might consist, for example, in forcing the Pekeris model with mean wind profiles typical of sPJOs, in order to test if the shifting of the resonance frequency toward the lunar period indeed occurs under these extreme wind conditions.

5. Conclusions

We have presented a detailed description of the response the MLT region exhibits during Northern Hemisphere wintertime extreme stratospheric events known as sPJOs. For this purpose, SMR wind measurements have been analyzed in combination with horizontal winds, GPHs, total ozone, and ozone concentration obtained from the 30-year nudged simulation by the Ext-CMAM30. The entire MLT region over Andenes (high latitude) and Juliusruh (middle latitude) is significantly disturbed during sPJO events, compared to other wintertime conditions. The observed mean winds and semidiurnal quasi-lunar (qM2) tide show clear enhancements that persist for several weeks after the CD of a sPJO event. The semidiurnal solar (S2) tide shows a decrease/increase pattern around the CD of sPJO events that is most likely due to changes in the mean zonal wind at mesospheric heights.

We have shown that the distinction between winters with or without major sudden stratospheric warmings is not sufficient and that a more detailed categorization into strong and non-PJO events, and winters with no major SSWs must be considered in order to explain the winter-to-winter variability of the MLT region. A clear example of this is that after a major SSW, the MLT wind and tidal behaviors strongly depend on the development (or not) of a sPJO event. In the absence of a sPJO event, the MLT winds and tides behave similar to a year with no major SSWs. On the other hand, after a sPJO event, intense jets develop in both components of the horizontal mean wind and the amplitudes of the semidiurnal tides enhance considerably, at both middle and high latitudes. GPH disturbances obtained from the Ext-CMAM30 show that after the CD of sPJOs, the polar vortex at stratospheric heights locates mainly over northern Europe. In the lower and middle mesosphere, it shifts toward Alaska and the North Pacific, and at upper mesospheric heights it splits into two parts, one of them being located over the North Atlantic European region and with its edge directly above Andenes and Juliusruh. This pattern is not detected during non-PJOs neither years with no MSSWs, which explains why the mean winds observed in the MLT during sPJO events exhibit significant differences with respect to the other two cases.

References

Andrews, D. G., Holton, J. R., & Leovy, C. B. (1987). *Middle atmosphere dynamics*. San Diego, California: Academic Press. https://doi.org/10.1002/qj.49711548612

Baldwin, M. P., & Dunkerton, T. J. (1999). Propagation of the arctic oscillation from the stratosphere to the troposphere. *Journal of Geophysical Research*, *104*, 30,937–30,946. https://doi.org/10.1029/1999JD900445

Butler, A. H., Sjoberg, J. P., Seidel, D. J., & Rosenlof, K. H. (2017). A sudden stratospheric warming compendium. *Earth System Science Data*, *9*, 63–76. https://doi.org/10.5194/essd-9-63-2017

Charlton, A. J., & Polvani, L. M. (2007). A new look at stratospheric sudden warmings. Part I: Climatology and modeling benchmarks. *Journal of Climate*, *20*, 449–469. https://doi.org/10.1175/JCLI3996.1

Charney, J. G., & Drazin, P. G. (1961). Propagation of planetary-scale disturbances from the lower into the upper atmosphere. *Journal of Geophysical Research*, *66*, 83–109. https://doi.org/10.1029/JZ066i001p00083

Chau, J. L., Fejer, B. G., & Goncharenko, L. (2009). Quiet variability of equatorial E × B drifts during a sudden stratospheric warming event. *Geophysical Research Letters*, *36*, L05101. https://doi.org/10.1029/2008GL036785

Chau, J. L., Hoffmann, P., Pedatella, N. M., Matthias, V., & Stober, G. (2015). Upper mesospheric lunar tides over middle and high latitudes during sudden stratospheric warming events. *Journal of Geophysical Research: Space Physics*, *120*, 3084–3096. https://doi.org/10.1002/2015JA020998

Conte, J. F., Chau, J. L., Laskar, F. I., Stober, G., Schmidt, H., & Brown, P. (2018). Semidiurnal solar tide differences between fall and spring transition times in the Northern Hemisphere. *Annales de Geophysique*, *36*, 999–1008. https://doi.org/10.5194/angeo-36-999-2018

Conte, J. F., Chau, J. L., Stober, G., Pedatella, N., Maute, A., Hoffmann, P., et al. (2017). Climatology of semidiurnal lunar and solar tides at middle and high latitudes: Interhemispheric comparison. *Journal of Geophysical Research: Space Physics*, *122*, 7750–7760. https://doi.org/10.1002/2017JA024396

de Grandpré, J., Beagley, S. R., Fomichev, V. I., Griffoen, E., McConnell, J. C., Medvedev, A. S., & Shepherd, T. G. (2000). Ozone climatology using interactive chemistry: Results from the Canadian Middle Atmosphere Model. *Journal of Geophysical Research*, *105*, 26,475–26,491. https://doi.org/10.5194/acp-14-1547-2014

Dee, D. P., Uppala, S. M., Simmons, A. J., Berrisford, P., Poli, P., Kobayashi, S., et al. (2011). The ERA-Interim reanalysis: Configuration and performance of the data assimilation system. *Quarterly Journal of the Royal Meteorological Society*, *137*, 553–597. https://doi.org/10.1002/qj.828

Fejer, B. G., Olson, M. E., Chau, J. L., Stolle, C., Lühr, H., Goncharenko, L. P., et al. (2010). Lunar dependent equatorial ionospheric electrodynamic effects during sudden stratospheric warmings. *Journal of Geophysical Research*, *115*, A00G03. https://doi.org/10.1029/2010JA015273

Fomichev, V., Ward, W. E., Beagley, S. R., McLandress, C., McConnell, J. C., McFarlane, N. A., & Shepherd, T. G. (2002). Extended Canadian Middle Atmosphere model: Zonal-mean climatology and physical parameterizations. *Journal of Geophysical Research*, *107*(D10), 4087. https://doi.org/10.1029/2001JD000479

Forbes, J. M. (1984). Middle atmosphere tides. *Journal of Atmospheric and Terrestrial Physics*, *46*(11), 1049–1067.

Forbes, J. M., & Zhang, X. (2012). Lunar tide amplification during the January2009 stratosphere warming event: Observations and theory. *Journal of Geophysical Research*, *117*, A12312. https://doi.org/10.1029/2012JA017963

Fritts, D. C., & Alexander, M. J. (2003). Gravity wave dynamics and effects in the middle atmosphere. *Reviews of Geophysics*, *41*(1), 1003. https://doi.org/10.1029/2001RG000106

Fuller-Rowell, T. J., Tzu-Wei, F., Wang, H., Matthias, V., Hoffmann, P., Hocke, K., & Studer, S. (2016). Impact of migrating tides on electrodynamics during the january 2009 sudden stratospheric warming. In T. FullerRowell, E. Yizengaw, P. H. Doherty, & S. Basu (Eds.), *In Ionospheric space weather* (Vol. 220). https://doi.org/10.1002/9781118929216.ch14

Fuller-Rowell, T. J., Wu, F., Akmaev, R., Fang, T.-W., & Araujo-Pradere, E. (2010). A whole atmosphere model simulation of the impact of a sudden stratospheric warming on thermosphere dynamics and electrodynamics. *Journal of Geophysical Research*, *115*, A00G08. https://doi.org/10.1029/2010JA015524

Goncharenko, L. P., Coster, A. J., Plumb, R. A., & Domeisen, D. I. V. (2012). The potential role of stratospheric ozone in the stratosphere-ionosphere coupling during stratospheric warmings. *Geophysical Research Letters*, *39*, L08101. https://doi.org/10.1029/2012GL051261

Goncharenko, L. P., & Zhang, S.-R. (2008). Ionospheric signatures of sudden stratospheric warming: Ion temperature at middle latitude. *Geophysical Research Letters*, *35*, L21103. https://doi.org/10.1029/2008GL035684

Harvey, V. L., Pierce, R. B., Fairlie, T. D., & Hitchman, M. H. (2002). A climatology of stratospheric polar vortices and anticyclones. *Journal of Geophysical Research*, *107*(D20), 4442. https://doi.org/10.1029/2001JD001471

Harvey, V. L., Randall, C. E., Goncharenko, L., Becker, E., & France, J. (2018). On the upward extension of the polar vortices into the mesosphere. *Journal of Geophysical Research: Atmospheres*, *123*, 9171–9191. https://doi.org/10.1029/2018JD028815

He, M., & Chau, J. L. (2019). Mesospheric semidiurnal tides and near-12 h waves through jointly analyzing observations of five specular meteor radars from three longitudinal sectors at boreal midlatitudes. *Atmospheric Chemistry and Physics*, *9*, 5993–6006.

He, M., Chau, J. L., Stober, G., Hall, C. M., Tsutsumi, M., & Hoffmann, P. (2017). Application of Manley-Rowe relation in analyzing nonlinear interactions between planetary waves and the solar semidiurnal tide during 2009 sudden stratospheric warming event. *Journal of Geophysical Research: Space Physics*, *122*, 10,783–10,795. https://doi.org/10.1002/2017JA024630

Hitchcock, P., Shepherd, T. G., & Manney, G. L. (2012). Statistical characterization of Arctic polar-night jet oscillation events. *Journal of Climate*, *26*, 2096–2116. https://doi.org/10.1175/JCLI-D-12-00202.1

Hocking, W., Fuller, B., & Vandepeer, B. (2001). Real-time determination of meteor-related parameters utilizing modern digital technology. *Journal of Atmospheric and Solar - Terrestrial Physics*, *63*(2-3), 155–169.

Hoffmann, P., Becker, E., Singer, W., & Placke, M. (2010). Seasonal variation of mesospheric waves at northern middle and high latitudes. *Journal of Atmospheric and Solar - Terrestrial Physics*, *72*(14-15), 1068–1079. https://doi.org/10.1016/j.jastp.2010.07.002

Hoffmann, P., Singer, W., Keuer, D., Hocking, W. K., Kunze, M., & Murayama, Y. (2007). Latitudinal and longitudinal variability of mesospheric winds and temperatures during stratospheric warming events. *Journal of Atmospheric and Solar - Terrestrial Physics*, *69*, 2355–2366. https://doi.org/10.1016/j.jastp.2007.06.010

Holton, J. R. (2004). *An introduction to dynamic meteorology* (4th ed.). San Diego, California: El-sevier Academic Press.

Jacobi, C., Kürschner, D., Muller, H., Pancheva, D., Mitchell, N., & Naujokat, B. (2003). Response of the mesopause region dynamics to the February 2001 stratospheric warming. *Journal of Atmospheric and Solar - Terrestrial Physics*, *65*, 843–855. https://doi.org/10.1016/S1364-6826(03)00086-5

Jin, H., Miyoshi, Y., Pancheva, D., Mukhtarov, P., Fujiwara, H., & Shinagawa, H. (2012). Response of migrating tides to the stratospheric sudden warming in 2009 and their effects on the ionosphere studied by a whole atmosphereionosphere model GAIA with COSMIC and TIMED/SABER observations. *Journal of Geophysical Research*, *117*, A10323. https://doi.org/10.1029/2012JA017650

Karpechko, A. Y., Hitchcock, P., Peters, D. H. W., & Schneidereit, A. (2017). Predictability of downward propagation of major sudden stratospheric warmings. *Quarterly Journal of the Royal Meteorological Society*, *143*, 1459–1470. https://doi.org/10.1002/qj.3017

Kodera, K., Kuroda, Y., & Pawson, S. (2000). Stratospheric sudden warmings and slowly propagating zonal-mean zonal wind anomalies. *Journal of Geophysical Research*, *105*, 12,351–12,359. https://doi.org/10.1029/2000JD900095

Kuroda, Y., & Kodera, K. (2004). Role of the polar-night jet oscillation on the formation of the Arctic oscillation in the Northern Hemisphere in winter. *Journal of Geophysical Research*, *109*, D11112. https://doi.org/10.1029/2003JD004123

Limpasuvan, V., Orsolini, Y. J., Chandran, A., Garcia, R. R., & Smith, A. K. (2016). On the composite response of the MLT to major sudden stratospheric warming events with elevated stratopause. *Journal of Geophysical Research: Atmospheres*, *121*, 4518–4537. https://doi.org/10.1002/2015JD024401

Lindzen, R. S., & Chapman, S. (1969). Atmospheric tides. *Space Science Reviews*, *10*, 3–188.

Liu, H.-L., & Roble, R. G. (2002). A study of a self-generated stratospheric sudden warming and its mesospheric-lower thermospheric impacts using the coupled TIME-GCM/CCM3. *Journal of Geophysical Research*, *107*(D23), 4695. https://doi.org/10.1029/2001JD001533

Manney, G. L., Zurek, R. W., ONeill, A., & Swinbank, R. (1994). On the motion of air through the stratospheric polar vortex. *Journal of the Atmospheric Sciences*, *51*, 2973–2994. https://doi.org/10.1175/1520-0469(1994)051h2973:OTMOATi2.0.CO;2

Matsuno, T. A. (1971). A dynamical model of the stratospheric sudden warming. *Journal of the Atmospheric Sciences*, *28*, 1479–1494.

Matthias, V., Hoffmann, P., Manson, A., Meek, C., Stober, G., Brown, P., & Rapp, M. (2013). The impact of planetary waves on the latitudinal displacement of sudden stratospheric warmings. *Annales de Geophysique*, *31*, 1397–1415. https://doi.org/10.5194/angeo-31-1397-2013

McCormack, J. P., Coy, L., & Singer, W. (2014). Intraseasonal and interannual variability of the quasi 2 day wave in the Northern Hemisphere summer mesosphere. *Journal of Geophysical Research: Atmospheres*, *119*, 2928–2946. https://doi.org/10.1002/2013JD020199

McLandress, C. (1997). Seasonal variability of the diurnal tide: Results from the Canadian middle atmosphere general circulation model. *Journal of Geophysical Research*, *102*, 29,747–29,764. https://doi.org/10.5194/acp-14-1547-2014

McLandress, C., Plummer, D. A., & Shepherd, T. G. (2014). Technical note: A simple procedure for removing temporal discontinuities in ERA-Interim upper stratospheric temperatures for use in nudged chemistry-climate model simulations. *Atmospheric Chemistry and Physics*, *14*, 1547–1555. https://doi.org/10.5194/acp-14-1547-2014

McLandress, C., Scinocca, J. F., Shepherd, T. G., Reader, M. C., & Manney, G. L. (2013). Dynamical control of the mesosphere by orographic and nonorographic gravity wave drag during the extended northern winters of 2006 and 2009. *Journal of the Atmospheric Sciences*, *70*, 2152–2169.

Mitchell, D. M., Charlton-Perez, A. J., & Gray, L. J. (2011). Characterizing the variability and extremes of the stratospheric polar vortices using 2D moment analysis. *Journal of the Atmospheric Sciences*, *68*, 1194–1213. https://doi.org/10.1175/2010JAS3555.1

Mitchell, D. M., Gray, L. J., Anstey, J., Baldwin, M. P., & Charlton-Perez, A. J. (2013). The influence of stratospheric vortex displacements and splits on surface climate. *Journal of Climate*, *26*, 2668–2682. https://doi.org/10.1175/JCLI-D-12-00030.1

Peters, D. H., Schneidereit, A., & Karpechko, A. Y. (2018). Enhanced stratosphere/troposphere coupling during extreme warm stratospheric events with strong polar-night jet oscillation. *Atmosphere*, *9*, 467.

Rossby, C.-G. (1939). Relation between variations in the intensity of the zonal circulation of the atmosphere and the displacements of the semipermanent centers of action. *Journal of Marine Research*, *2*, 38–55.

Runde, T., Dameris, M., Garny, H., & Kinnison, D. E. (2016). Classification of stratospheric extreme events according to their downward propagation to the troposphere. *Geophysical Research Letters*, *43*, 6665–6672. https://doi.org/10.1002/2016GL069569

Scinocca, J. F., McFarlane, N. A., Lazare, M., Li, J., & Plummer, D. (2008). The CCCma third generation AGCM and its extension into the middle atmosphere. *Atmospheric Chemistry and Physics*, *8*, 7055–7074. https://doi.org/10.5194/acp-8-7055-2008

Siddiqui, T. A., Maute, A., Pedatella, N., Yamazaki, Y., Lühr, H., & Stolle, C. (2018). On the variability of the semidiurnal solar and lunar tides of the equatorial electrojet during sudden stratospheric warmings. *Annales de Geophysique*, *36*, 1545–1562. https://doi.org/10.5194/angeo-2018-80

Siegmund, P. (2005). Stratospheric polar cap mean height and temperature as extended-range weather predictors. *Monthly Weather Review*, *133*, 2436–2448. https://doi.org/10.1175/MWR2985.1

Stober, G., Chau, J. L., Vierinen, J., Jacobi, C., & Wilhelm, S. (2018). Retrieving horizontally resolved wind fields using multi-static meteor radar observations. *Atmospheric Measurement Techniques*, *11*, 4891–4907.

Stober, G., Matthias, V., Jacobi, C., Wilhelm, S., Höffner, J., & Chau, J. L. (2017). Exceptionally strong summer-like zonal wind reversal in the upper mesosphere during winter 2015/16. *Annales de Geophysique*, *35*, 711–720.

Waugh, D., & Randel, W. (1999). Climatology of Arctic and Antarctic polar vortices using elliptical diagnostics. *Journal of the Atmospheric Sciences*, *56*, 1594–1613. https://doi.org/10.1175/1520-0469(1999)056h1594:COAAAPi2.0.CO;2

Wilhelm, S., Stober, G., & Chau, J. L. (2017). A comparison of 11-year mesospheric and lower thermospheric winds determined by meteor and MF radar at 69°N. *Annales de Geophysique*, *35*, 893–906. https://doi.org/10.5194/angeo-35-893-2017

Yiğit, E., & Medvedev, A. S. (2015). Internal wave coupling processes in Earth's atmosphere. *Advances in Space Research*, *55*, 983–1003. https://doi.org/10.1016/j.asr.2014.11.020

Zhang, X., & Forbes, J. M. (2014). Lunar tide in the thermosphere and weakening of the northern polar vortex. *Geophysical Research Letters*, *41*, 8201–8207. https://doi.org/10.1002/2014GL062103

Zülicke, C., Becker, E., Matthias, V., Peters, D. H. W., Schmidt, H., Liu, H.-Li, et al. (2018). Coupling of stratospheric warmings with mesospheric coolings in observations and simulations. *Journal of Climate*, *31*, 1107–1133. https://doi.org/10.1175/JCLI-D-17-0047.1

Zülicke, C., & Peters, D. H. W. (2008). Parameterization of strong stratospheric inertia gravity waves forced by poleward-breaking ross by waves. *Monthly Weather Review*, *136*(1), 98–119. https://doi.org/10.1175/2007MWR2060.1